Isomeric Solid Additive Enables High-Efficiency Polymer Solar Cells Developed Using a Benzo-difuran-based Donor Polymer

Lu Chen, Jicheng Yi, Ruijie Ma*, Lu Ding, Top Archie Dela Peña, Heng Liu, Jian Chen, Cuifen Zhang, Chaoyue Zhao, Wen Lu, Qi Wei, Bin Zhao, Huawei Hu, Jiaying Wu, Zaifei Ma, Xinhui Lu, Mingjie Li, Guangye Zhang*, Gang Li*, He Yan*

Lu Chen, Chaoyue Zhao, Prof. Guangye Zhang
College of New Materials and New Energies, Shenzhen Technology University, Shenzhen 518118, China
Email: zhangguangye@sztu.edu.cn

Lu Chen, Dr. Jicheng Yi, Top Archie Dela Peña, Prof. He Yan
Department of Chemistry Department of Chemistry and Hong Kong Branch of Chinese National Engineering Research Center for Tissue Restoration and Reconstruction, The Hong Kong University of Science and Technology, Clear Water Bay, Hong Kong, China
Email: hyan@ust.hk

Dr. Ruijie Ma, Prof. Gang Li
Department of Electronic and Information Engineering, Research Institute for Smart Energy (RISE), Guangdong-Hong Kong-Macao (GHM) Joint Laboratory for Photonic-Thermal-Electrical Energy Materials and Devices, The Hong Kong Polytechnic University, Hung Hom, Kowloon, Hong Kong, 999077, China
Email: ruijie.ma@polyu.edu.hk; gang.w.li@polyu.edu.hk

Top Archie Dela Peña, Dr. Qi Wei, Prof. Mingjie Li
Department of Applied Physics, The Hong Kong Polytechnic University, Hong Kong, China

Heng Liu, Prof. Xinhui Lu
Department of Physics, The Chinese University of Hong Kong, Hong Kong, Shatin 999077 Hong Kong, China

Dr. Lu Ding, Dr. Jian Chen, Prof. He Yan
Hong Kong University of Science and Technology Fok Ying Tung Research Institute, S&T Building, Nansha IT Park, Guangzhou City, 511458, P. R. China

Cuifen Zhang, Prof. Zaifei Ma, Prof. Huawei Hu
State Key Laboratory for Modification of Chemical Fibers and Polymer Materials, Center for Advanced Low-dimension Materials, College of Materials Science and Engineering, Donghua University, Shanghai, 201620 China

Top Archie Dela Peña, Prof. Jiaying Wu
The Hong Kong University of Science and Technology, Function Hub, Advanced Materials Thrust, Nansha 511400, Guangzhou, P.R. China

Wen Lu, Prof. Bin Zhao
Key Laboratory of Polymeric Materials & Application Technology of Hunan Province
College of Chemistry, Xiangtan University, Xiangtan 411105, P. R. China

Prof. He Yan
eFlexPV Limited (Foshan), Guicheng Street, Nanhai District, Foshan 528200, China

Abstract

Currently, nearly all high-efficiency organic photovoltaic devices use donor polymers based on the benzo-dithiophene (BDT) unit. To diversify the choices of building blocks for high-performance donor polymers, we explored the use of benzo-difuran (BDF) units, which could achieve reduced steric hindrance, stronger molecular packing, and tunable energy levels. In previous research, the performances of BDF-based devices lagged behind those of BDT-based devices. In this study, we achieved a high efficiency (18.4%) using a BDF-based polymer donor, which is the highest efficiency reported for BDF donor materials to date. The high efficiency is enabled by a donor polymer (D18-Fu) and the aid of a solid additive (2-chloronaphthalene), which is the isomer of the commonly used additive 1-chloronaphthalene. Our results revealed the significant effect of 2-chloronaphthalene in optimizing the morphology and enhancing the device parameters. Our work not only provides a new building block that can achieve an efficiency comparable to dominant BDT units but also proposes a new solid additive that could replace the widely used 1-chloronaphthalene additive.

Key words: benzo[1,2-b:4,5-b′]difuran, organic solar cells, power conversion efficiency, isomeric solid additive

Introduction

Benzo [1,2-b:4,5-b′]difuran (BDF) building block-based polymer donor materials are promising for pursuing high power conversion efficiencies (PCEs) of organic solar cells (OSCs), thus promoting commercialization. Compared to the widely adopted benzo[1,2-b:4,5-b′]dithiophene (BDT) building block, the BDF unit is smaller in size and could thus reduce steric hindrance, which typically leads to closer molecular packing and greater charge carrier mobility.[1] Furan is bio-renewable and is more eco-friendly than thiophene, which is beneficial for large-scale synthesis and recycling.[2] However, the highest leading PCEs (>19%) are currently achieved by BDT polymer donors, while BDF-based devices have achieved highest PCEs of ~17%.[3-12] To accelerate the improvement of the PCE of BDF-based OSCs, chemical and device engineering efforts should be carried out, as was conducted for BDT-based OSCs.[13-21]

Suitable device engineering can significantly enhance the performance of a given material system. Compared with BDT-based polymer donors, whose material and device performances have been extensively studied, the progress of BDF-based systems has mainly been driven by material design, leaving great space for improvements from device engineering. For instance, we recently demonstrated an efficient BDF polymer named D18-Fu, which achieved a PCE of 16.38% with Y6-1O, and further increased the PCE to 17.07% using fullerene as the third component in the ternary strategy.[11] However, that was only our first attempt. As the structure-performance relationship suggests, when a new backbone is introduced, the characteristics of the polymer and its performance in an organic photovoltaic device can vary. Therefore, we believe that novel BDF polymers can realize top-of-the-line PCEs with proper device engineering .

Herein, we demonstrate an 18.4% PCE achieved using D18-Fu. We constructed the active layer using a combination of D18-Fu and L8-BO and incorporated 2-chloronaphthalene (2-CN), the isomeric solid additive of one of the most commonly used solvent additives, 1-chloronaphthalene (1-CN), to tune the film morphology.[11, 22-23] The mechanism of 2-CN was compared with 1-CN and without additive using in-situ absorption. We show that by changing the appearance order and speed of the donor and acceptor main/associate peaks, 2-CN helps realize the most desired molecular packing, crystallinity, phase separation, and vertical composition distribution, leading to minimized energy loss, especially compared to the 1-CN based counterpart, as well as favorable device physics characteristics. Furthermore, theoretical calculations revealed that the interaction between 2-CN and L8-BO leads to an enhanced dipole moment perpendicular to the acceptor molecular plane, thus enabling faster nucleation and crystallization of the acceptor. To prove the generality of 2-CN as an effective additive, we evaluated the performance of 2-CN in two other well-known systems, PM6:Y6 and PM6:PY-IT, where 1-CN has been shown to be fundamentally important in their performance optimization. The results demonstrate that 2-CN is slightly better than 1-CN in these systems, indicating that the structure-induced morphology formation in D18-Fu:L8-BO is largely different from that in PM6-based systems.

Results and Discussion

D18-Fu and L8-BO were synthesized according to the literature and were of similar quality, whereas 1-CN and 2-CN were commercially available and were used without further purification. The chemical structures of D18-Fu and L8-BO, including the polymer donor, small-molecule acceptor, and additives, are presented in **Figure 1a**. 2-CN had a slightly higher polarity than 1-CN, which changes the interaction between the additive and photovoltaic materials, producing an additional route to realize improved thin-film morphology.[24-26] In addition, solid 2-CN can be better transported than liquid 1-CN.

First, the photovoltaic performance of the isomeric additive strategy upon the BDF-based system was investigated by fabricating a series of conventional structural devices of ITO/PEDOT:PSS-TA[27]/D18-Fu:L8-BO/PNDIT-F3N/Ag. The current density versus voltage (*J-V*) characteristics of the best devices for three different conditions are shown in **Figure 1b**, with the summarized parameters in **Table 1**. The untreated precursor-based devices achieved a 17.4% efficiency, which is higher BDF-type counterparts, highlighting the importance of material selection for finding the best donor-acceptor combination. 1-CN processed devices displayed improved short-circuit current density (J_{SC}) and fill factor (*FF*), resulting in a slightly enhanced efficiency of 17.8%. However, the open-circuit voltage (V_{OC}) experienced some loss. The highest PCE was attained by the 2-CN pre-processed devices, which maintained their V_{OC} and exhibited a $J_{SC}\times FF$ value similar to that of their 1-CN counterparts. These advantages resulted in a PCE of 18.4%, a breakthrough for BDF-unit-based polymer solar cells. To understand this achievement, the efficiencies of this study and other studies are summarized in **Figure 1c**. As indicated, previous advancements were mostly driven by chemical inputs, that is, the production of new materials, whereas device engineering has received less attention. In contrast, our work, in conjunction with our previous report, has elevated the PCE to a new level by combining chemical and device efforts. Specifically, we synthesized new materials, rationally selected donor-acceptor combinations, and applied an innovative morphology tuning strategy using isomeric additives. The details are summarized in **Table S1**. The device parameters were

extracted from 20 independent results for each system and their normal distribution is depicted in **Figure 1d** and **S1**. Additionally, we measured the external quantum efficiency (EQE) spectra of the optimal devices to confirm the reliability of *the J-V* results. As shown in **Figure 1e**, with the integrated current density values in **Table 1**, we controlled the error to be less than 3%.

The device stability under standard illumination in an operational environment was studied by placing encapsulated solar cells under a simulated 1-sun LED in air.[28-30] As shown in **Figure S2**, and summarized in **Table S2**, in a five day period, the 2-CN treated device better maintained the PCE, suggesting that the isomeric solid additive tactic has the potential to improve device stability.

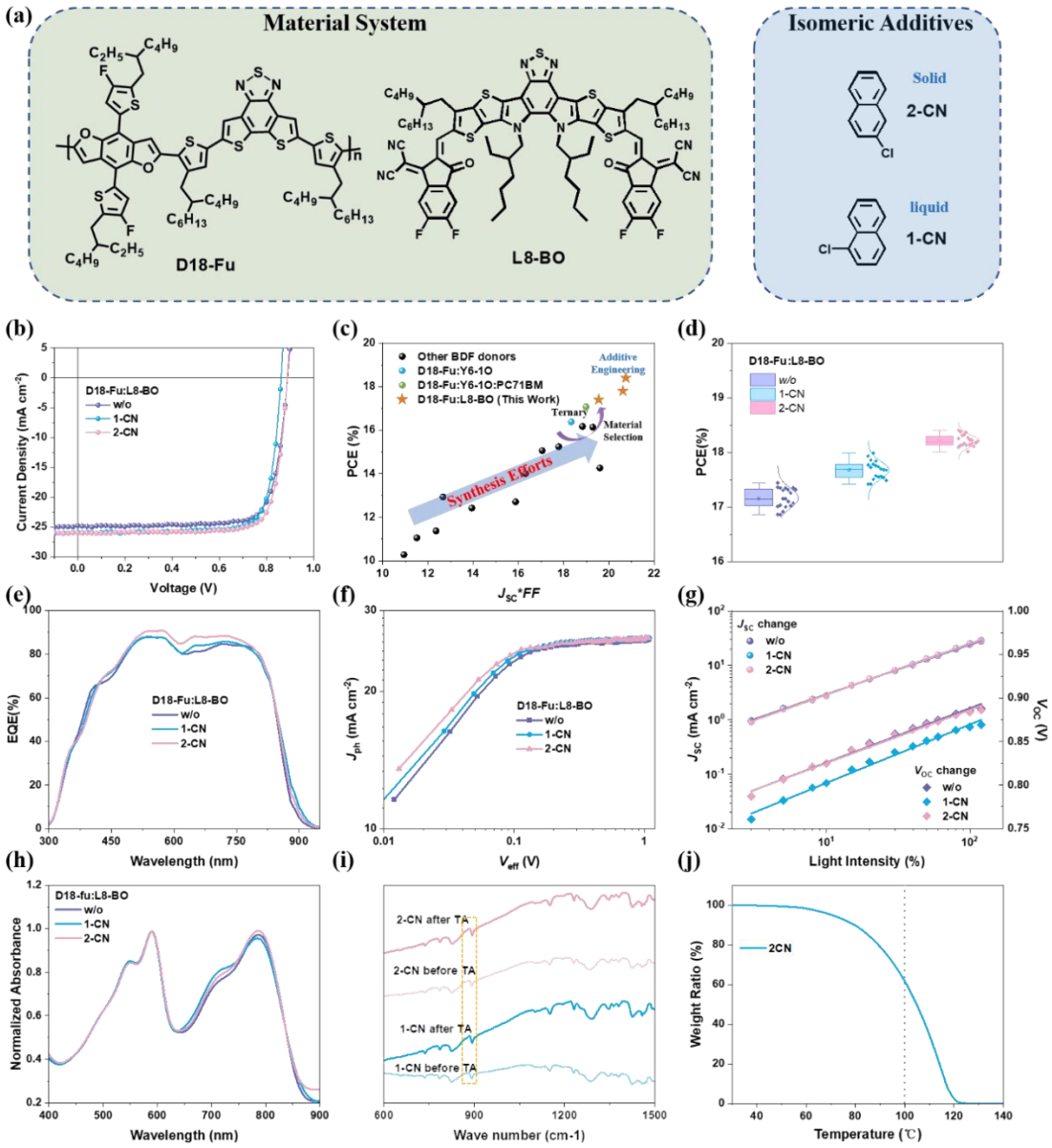

Figure 1. (a) Chemical structures of photovoltaic materials and isomeric additives. (b) *J-V* characteristics. (c) Summary of the performance of BDF polymer based OSCs with over 10% efficiency. (d) Normal distributions of PCEs for 20 independent device. (e) The EQE spectra. (f) J_{ph}-V_{eff} relationships. (g) J_{SC}/V_{OC} against light intensity. (h) UV-vis absorption. (i) FT-IR spectra. (j) TGA curves of the 2-CN samples.

Table 1. Device performances.

D18-Fu:L8-BO	V_{OC} (V)	J_{SC} (mA cm^{-2})	*FF* (%)	PCE (%)
w/o	0.887(0.892±0.009)	24.9(24.5±0.8)/24.7	78.5(78.3±1.4)	17.4 (17.1±0.2)
1-CN	0.861(0.871±0.006)	25.9(25.4±0.4)/25.1	79.6(79.7±0.6)	17.8 (17.7±0.2)
2-CN	0.886(0.887±0.004)	26.0(25.9±0.3)/25.6	79.8(79.2±0.7)	18.4 (18.2±0.1)

The brackets contain averages and standard deviation of PCEs based on 20 devices.

Companion device physics studies were performed: photocurrent density (J_{ph}) vs. effective voltage (V_{eff}) relationships and J_{SC}/V_{OC} vs light intensity curves (**Figure 1f-1g**). The details of the mechanism and derivation can be found in the ***Supporting Information***. The results showed that the additive treatment promoted the charge generation efficiency from 96.0% to 99.2% and 99.5%, and the 2-CN device had a clearly higher charge collection efficiency of 90.9% (89.8% for 1-CN, 88.5% for *w/o*). The *S* values calculated from *the* J_{SC} variation were 0.913, 0.934, and 0.935, respectively, indicating that bimolecular recombination was suppressed by isomeric additives. The ideal factor *n*s were 1.04, 1.12, and 1.02 respectively, according to V_{OC}'s change in VOC, which implies that trap-assisted recombination regains some dominance in the 1-CN processed device after bimolecular recombination is suppressed but is reduced by 2-CN treatment.

The device performance differences in the *w/o*, 1-CN, and 2-CN devices differed in terms of V_{OC}, J_{SC} and *FF*. Therefore, the film morphology tuning process should be carefully studied to precisely determine the underlying structure-property-performance relationship. First, we evaluated the general optical characteristics via ultraviolet-visible (UV-vis) spectroscopy, as illustrated in **Figure 1h**. This revealed that D18-Fu's aggregation was not clearly affected by solvent/solid isomeric additives, which is probably attributed to its strong pre-aggregation in the solution state, similar to other high-performance polymeric donor materials.[31-36] Therefore, polymer-formed fibrillar networks that are favorable for charge separation and transport were present in all films. The main differences were found in the acceptor (L8-BO) region. Relatively, the intensity of the 0-1 vibrational peak was promoted by 1-CN treatment and that of the 0-0 peak was weakened. Simultaneously, the 2-CN processed film generally improved the 0-1 and 0-0 peaks. These phenomena suggest that the morphology (crystallinity + phase separation) differs depending on the isomeric additive. The film morphology was first determined by the drying process during spinning and post treatment (thermal annealing; TA). The volatility of 1-CN and 2-CN is of great importance in this scenario. Next, the films with additives before and after TA were analyzed using Fourier-transformed infrared spectroscopy (FTIR). As depicted in **Figure 1i**, the difference in

signal intensity was negligible; therefore, 1-CN and 2-CN likely evaporated during spinning.[37] This is supported by the thermogravimetric analysis (TGA) curve of 2-CN in **Figure 1j**, which is similar to 1-CN and naphthalene, representing their generally identical volatile properties.[37,38]

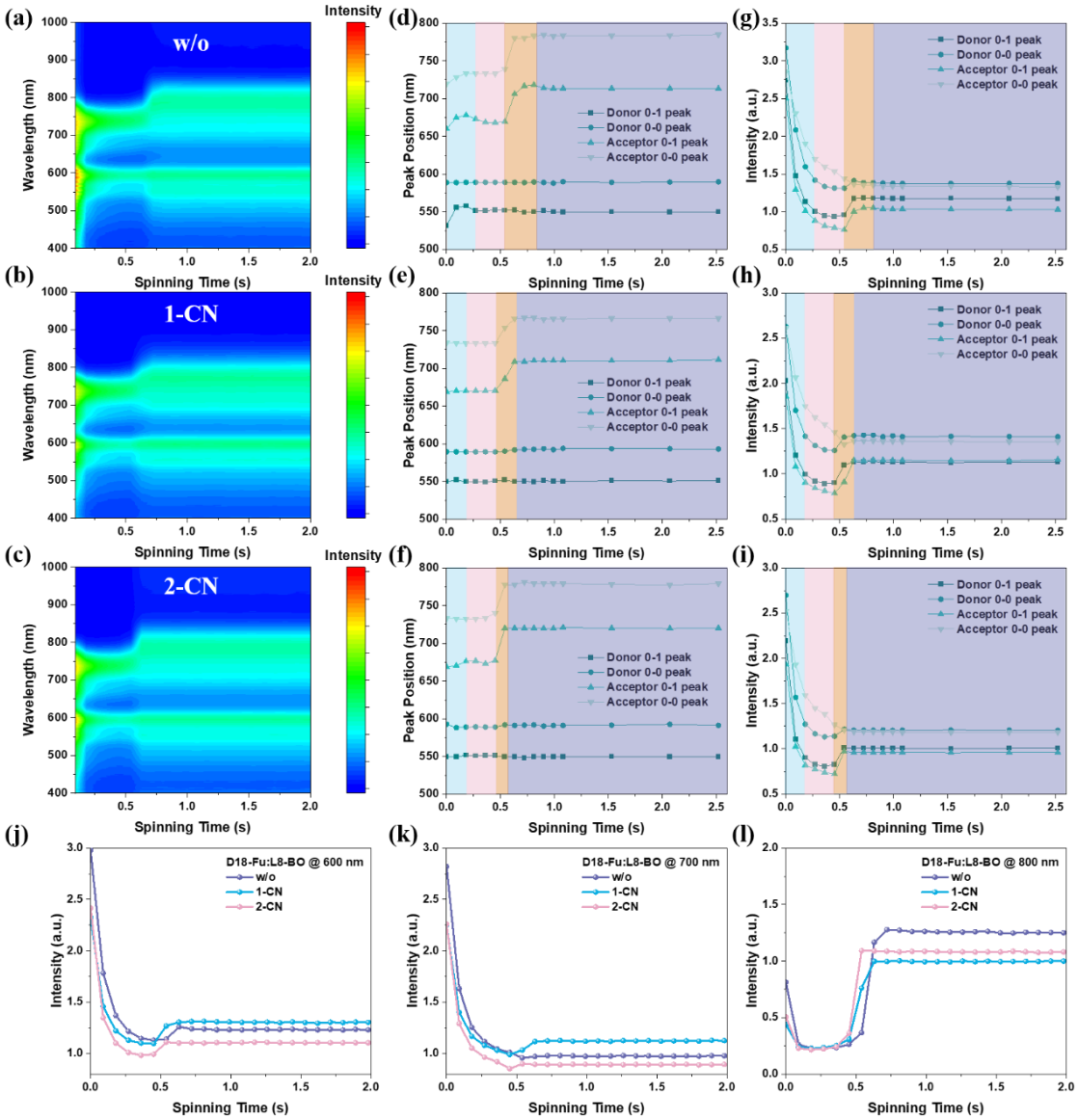

Figure 2. *In situ* UV-vis absorption study: 2D contour maps of (a) w/o, (b) 1-CN, and (c) 2-CN type solution-to-film process absorption. Positions of 0-1 and 0-0 peaks for donor and acceptor in films of (d) w/o, (e) 1-CN, and (f) 2-CN types. Peak intensity changes of 0-1 and 0-0 peaks for donor and acceptor in films of (g) w/o, (h) 1-CN, and (i) 2-CN categories. Absorption intensity of three types of films variation tendency by time at (j) 600 nm, (k) 700 nm, and (l) 800 nm.

Since general characterizations cannot determine the film drying mechanism, a

powerful tool called *in situ* UV-vis was utilized.[39-42] The contour maps of the absorption spectra of the three types of films during the drying process are shown in **Figure 2a-2c** and the positions and intensities of the 0-0 & 0-1 peaks in the donor and acceptor regions are shown in **Figure 2d-2i**, from which four stages of film formation within 2 s can be recognized. In 1st, 2nd, and 3rd stages (colored blue, pink, and orange, respectively), solvent removal was completed; thus, in the purple range, the peak position and intensity were constant. The whole process of D18-Fu:L8-BO systems was divided based on the intensity variation: the blue part with a fast decrease in intensity represents the removal of chloroform (liquid to solid); the pink region with a slower intensity reduction is mainly caused by a decrease in film thickness due to the centrifugation effect; and the orange period is generated by the aggregation of L8-BO (D18-Fu is mainly pre-aggregated). The use of 1-CN and 2-CN accelerated the speed of L8-BO aggregation (faster intensity enhancement and peak position red shift), which could be beneficial to forming a high-crystallinity pure acceptor phase, and thus boosted charge transport. Interestingly, isomeric additives did not impact the length of solvent removal and film thinning duration but a slight pre-redshift of acceptor peaks was observed for 2-CN processed systems, indicating that its volatile nature could be more significant than that of 1-CN. Meanwhile, isomeric additives can stabilize the peak position fluctuation of the donor's 0-1 peak, meaning a more controllable polymer pre-aggregation is achieved. However, the rise of the acceptor 0-1 peak of the 1-CN processed film was the longest, meaning that the H-aggregation of L8-BO was very much induced by it, while the other two systems were shorter, which is consistent with the steady-state UV-vis spectra. The absorbance of the different systems at 600, 700, and 800 nm were traced over time, as portrayed in **Figure 2j-2l**. The results confirmed the faster aggregation due to the additives. The 600 nm absorbance variation reflects that D18-Fu's full assembly is faster, so pre-aggregation of the polymer donor might be enhanced by 1-CN and 2-CN. The 700 nm tracing supports that 1-CN can significantly increase the H-aggregation of L8-BO, consistent with our previous deduction. For 800 nm, the lower absorbance of the additive-processed films after solidification implies that the corresponding films have narrower peak widths; therefore, a more ordered

molecular packing is expected. In short, 2-CN results in a film formation process of simultaneous donor-acceptor crystallization, possibly reaching multilength-scale phase separation behavior after solidification, which is thought to be the fundamental reason for efficient charge generation and transport.[43]

The UV-vis absorption of the neat donor and acceptor films with different treatments supported the above findings. As shown in **Figure S3**, the H-aggregation of L8-BO was significantly enhanced by 1-CN treatment. 2-CN caused a redshift for the 0-0 peak; however, this does not necessarily lead to a redshift of the EQE spectrum for 2-CN treated devices, since the crystallization of L8-BO would be suppressed by the existence of D18-Fu, as supported by the blend film UV-vis absorption profiles. Meanwhile, both CN additives slightly suppressed the H-aggregation of D18-Fu, which could be beneficial for improving conjugation and thus better hole transport.

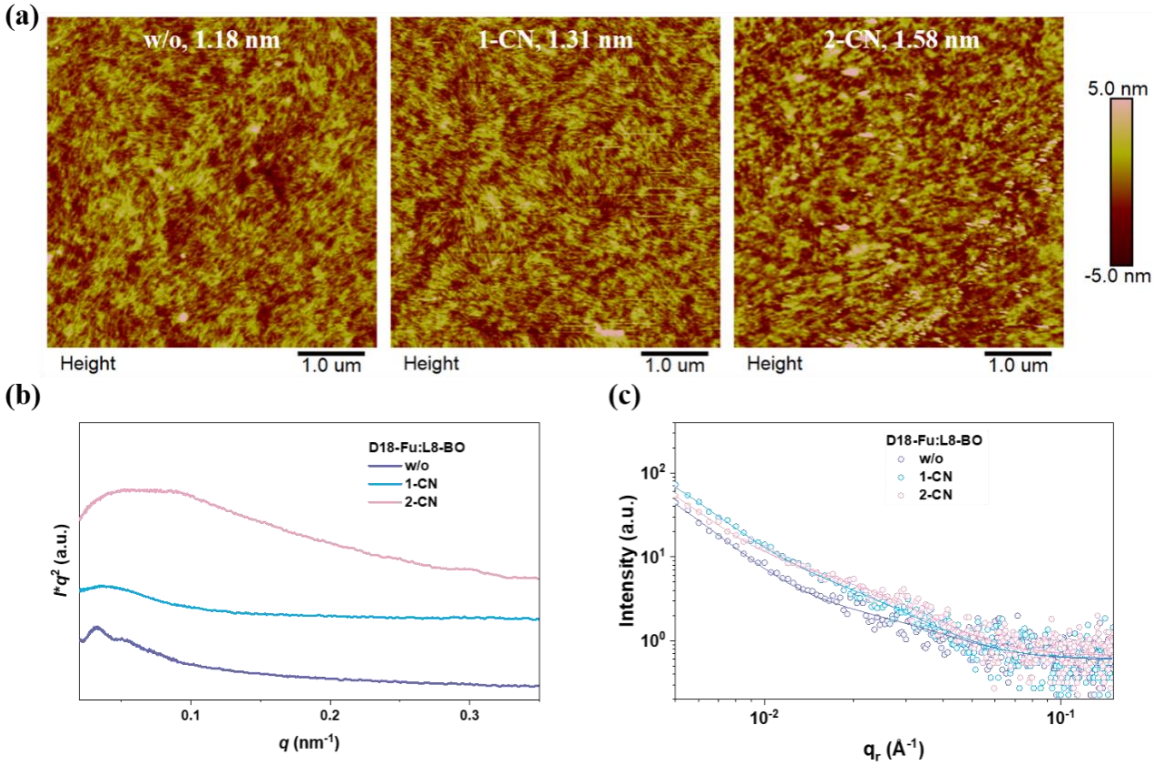

Figure 3. Morphology study: (a) Atomic force spectroscopy height images of three kinds of active layers. (b) Resonant soft X-ray scattering results. (c) grazing-incidence small-angle X-ray scattering in-plane (IP) plots and fitting lines.

Following the real-time investigation of the solution-to-film process, the next target

was to observe the film morphology after spinning and post-treatment. The general features were evaluated using atomic force spectroscopy measurements. The height images are presented in **Figure 3a**, noting the surface roughness values of them are 1.18 nm, 1.31 nm and 1.58 nm, respectively, consistent to the prediction 2-CN induces the strongest aggregation. Then, resonant soft X-ray scattering technology was utilized for quantitative analysis of the domain size and relative purity.[44-46] The test results are shown in **Figure 3b**. *w/o* and 1-CN active layers exhibited only long-scale domain sizes of 92.5 and 87.3 nm, respectively, while 2-CN treated D18-Fu:L8-BO film exhibited large and small domains with sizes of 65.4 nm and 31.1 nm. In addition, the relative purity values of large-scale domains for *w/o*, 1-CN, and 2-CN films were 25.6%, 17.8%, and 100%, respectively. This implies that 2-CN results in multilength-scale phase separation behavior, which is consistent with the hypothesis proposed above. On the other hand, grazing-incidence small-angle X-ray scattering was used to evaluate the length scale of the pure acceptor phase and mixing phase to confirm the phase segregation.[47,48] The 2D patterns are presented in **Figure S4** and the in-plane (IP) intensity profiles are plotted in **Figure 3c**, together with the corresponding fitting lines. The length scale of the pure phase ($2Rg$) and intermixing region (X_{DAB}) values were 11/26, 16/30, and 16/25 nm, respectively. These results are consistent with the domain purity increase in the 2-CN treated active layer. In addition, the rise in the pure acceptor phase in the solid isomeric additive system detected here also supports the multilength-scale morphology feature.

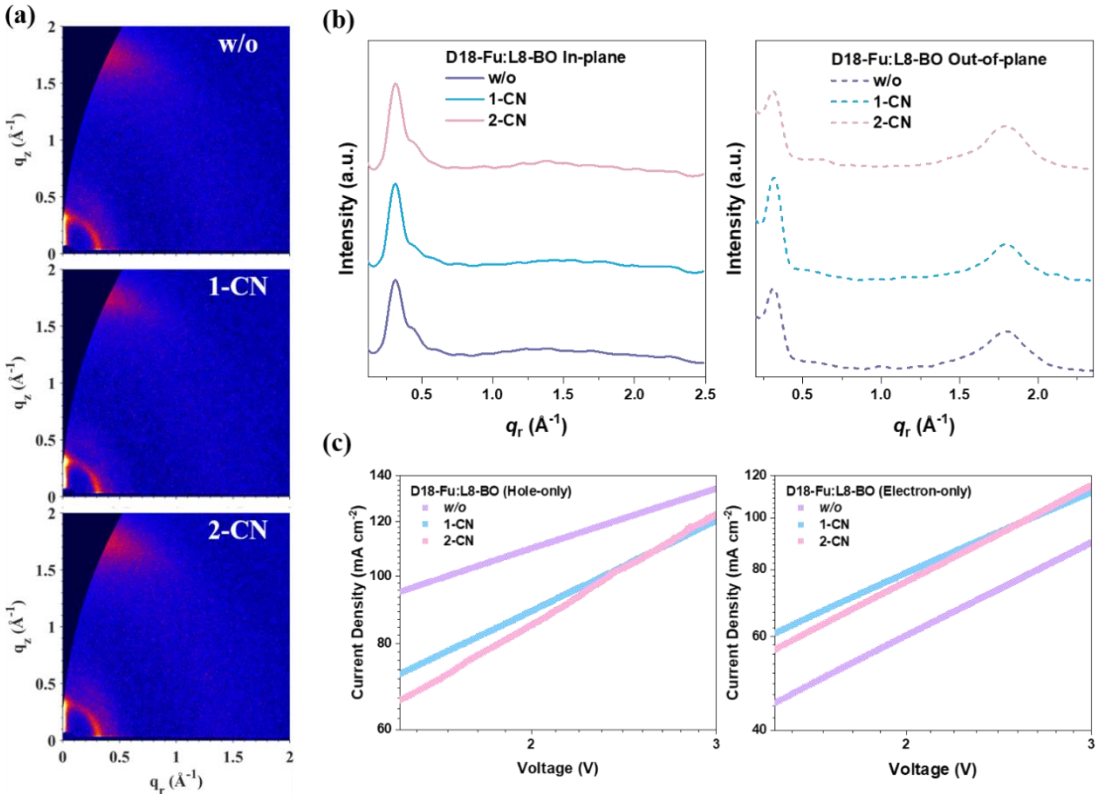

Figure 4. (a) 2D GIWAXS patterns. (b) IP and OOP line-cuts for D18-Fu:L8-BO series. (c) Hole-only and electron-only device results.

The molecular packing and crystallinity tuning effect of isomeric additives were studied via grazing incidence wide-angle X-ray scattering (GIWAXS) tests.[49-51] The 2D patterns, relative line-cuts, and calculated peak parameters along the IP and out-of-plane (OOP) directions are displayed in **Figure 4a-4b** and **Table S3**, **S4**. The lamellar chain packing diffraction was co-contributed by D18-Fu and L8-BO, whose peaks can be found at 0.31and 0.44 Å^{-1}, respectively. The independent lamellar packing peak position for L8-BO was at ~ 0.51 Å^{-1};[23] thus the blending between donor and acceptor in film is a semi-intermixing state in a long-distance packing motif. As for OOP direction, two peaks appeared at 0.31 and 1.79 Å^{-1}: the lamellar packing signal of D18-Fu was perpendicular to the substrates and L8-BO's π-π stacking diffraction. Therefore, the compressed π-π stacking d-spacing value from 3.70 to 3.53 Å is caused by D18-Fu, while the additive processing tunes the coherence lengths from 31.0 Å to 34.7 and 27.3 Å. Although the π-π region analysis suggests a less ordered stacking for L8-BO in the short distance induced by 2-CN, its strongest diffraction signal supports an improved general crystallinity. This feature could lead to a well-maintained bandgap and V_{OC}, as

well as a favorable charge transport ability (for *FF*). A space charge limited current (SCLC) method was applied to evaluate the hole and electron mobilities (μ_h & μ_e) of the D18-Fu:L8-BO systems. The *J-V* curves of the hole-only and electron-only devices are plotted in **Figure 4c**. The corresponding μ_h & μ_e values for each system were 2.8×10^{-4} $cm^2V^{-1}s^{-1}$ and 3.2×10^{-4} $cm^2V^{-1}s^{-1}$, 3.6×10^{-4} $cm^2V^{-1}s^{-1}$ and 4.2×10^{-4} $cm^2V^{-1}s^{-1}$, 4.9×10^{-4} $cm^2V^{-1}s^{-1}$ and 5.3×10^{-4} $cm^2V^{-1}s^{-1}$, respectively. Interestingly, a lower CL value did not lead to an inferior μ_e for the 2-CN treated active layer, which is probably due to its enhanced μ_h accelerate the electron transport. Charge transport is a complex process dependent on many factors.

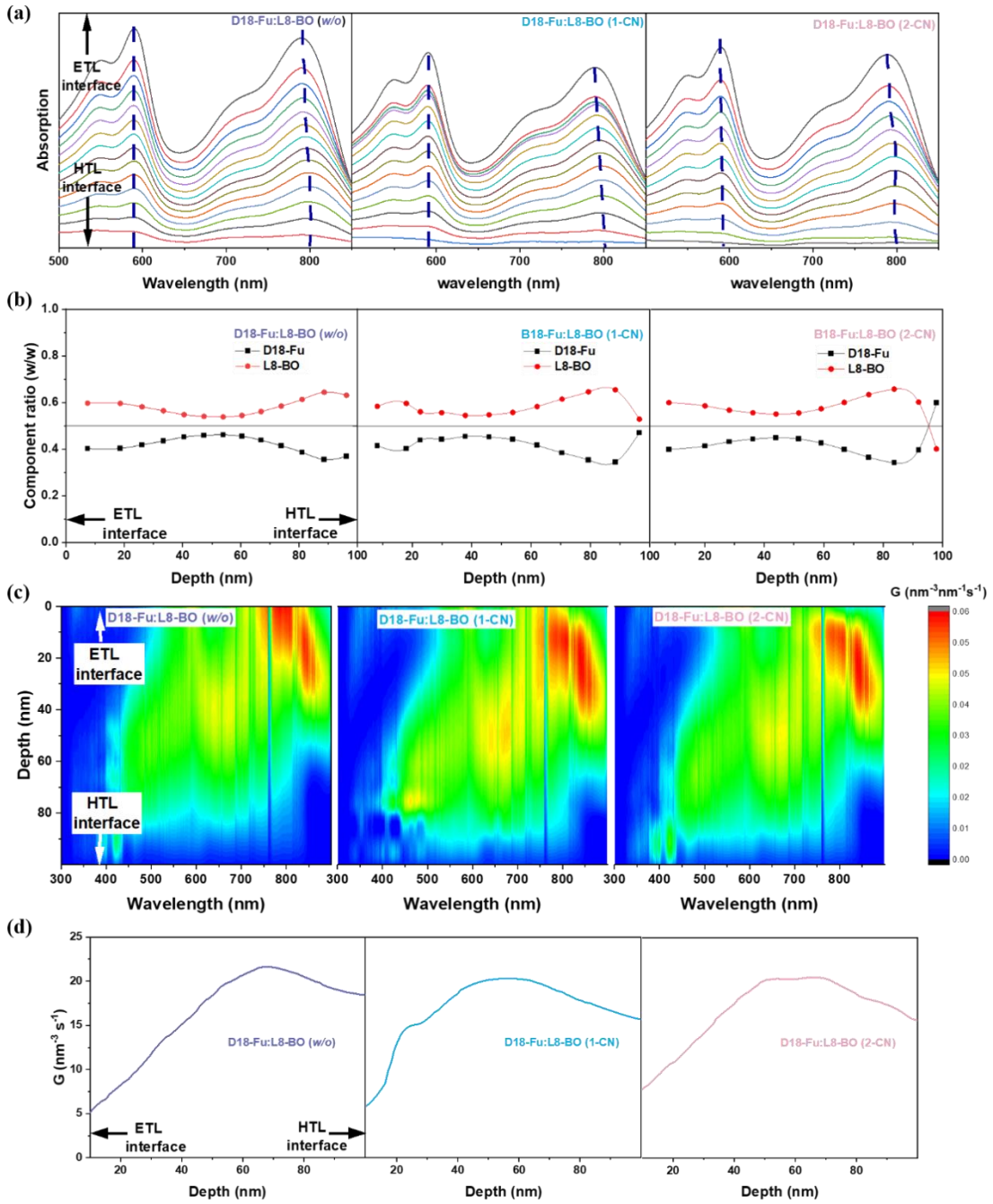

Figure 5. (a) Film-depth-dependent absorption spectroscopy. (b) Derived D18-Fu vs L8-BO weight ratio vertical distribution. (c) Calculated exciton generation contours. (d) Integration of exciton production rate with respect to depth.

The vertical segregation of D18-Fu and L8-BO tuned by isomeric additives was studied using film-depth-dependent light absorption spectroscopy characterization.[52-54] The results are presented in **Figure 5a** and the composition weight ratio of D18-Fu and L8-BO, charge generation heat maps, and integrated curves are provided in **Figure 5b-5d,** respectively**.** The *w/o* film exhibited an averaged vertical distribution in the

medium level and somewhat L8-BO rich regions at the bottom and upper levels. The 1-CN treatment takes the averaged interpenetrating part to a shallower place, and the main acceptor-rich distribution approaches the bottom. However, the ratio of D18-Fu was at the deepest level, which is beneficial to suppressing the charge recombination before charge collection. In the 2-CN enabled system, the D18-Fu enrichment at the bottom was more significant than that in the 1-CN system, while the other region's weight ratio curves were similar. This supports the slightly higher *FF* achieved for the 2-CN system. The charge generation distribution results substantiate that the H-aggregation driven by 1-CN is the strongest, and that from 2-CN is medium. In addition, this implies that the free charge is almost fully generated in the 2-CN film, thus providing the best J_{SC}.

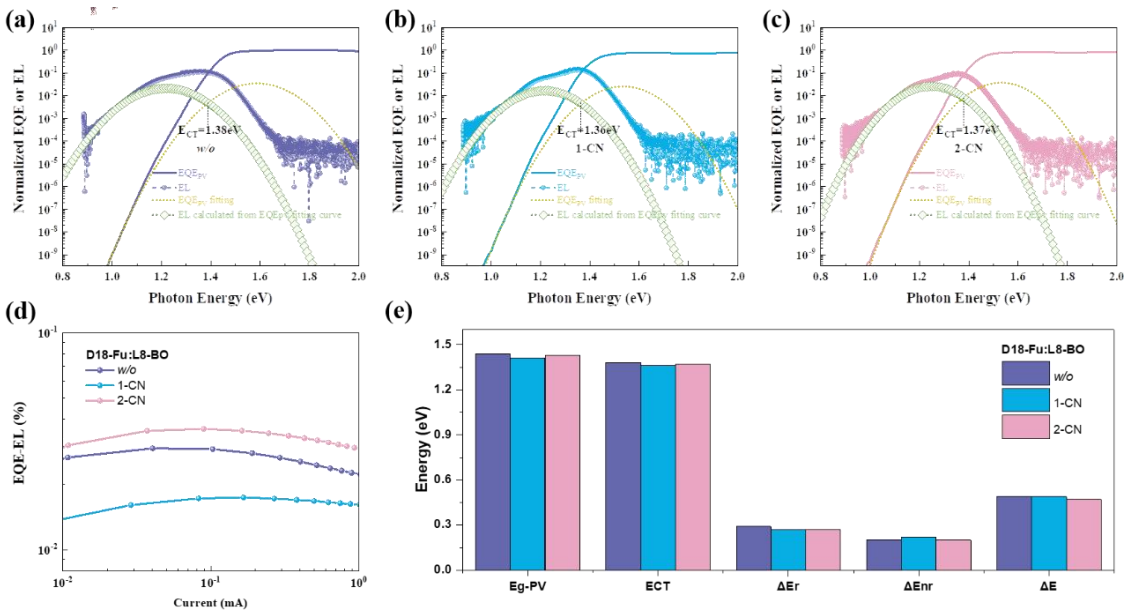

Figure 6. Energy loss analysis. Marcus fitting for D18-Fu:L8-BO solar cells of (a) w/o, (b) 1-CN and, (c) 2-CN treatment. (d) EQE-electroluminescence (EL) results. (e) Calculated result summary.

After addressing the morphological evolution-induced J_{SC} and *FF* change, the well-maintained V_{OC} in the 2-CN type device was further investigated. Accordingly, Fourier-transform photocurrent spectroscopy external quantum efficiency and external quantum efficiency electroluminescence (EQE-EL) measurements were carried out.[55-57] The results, including the Marcus theory supported charge transfer (CT) energy state

analysis and non-radiative loss assessment based on EQE-EL, are presented in **Figure 6a-6d**. A calculation summary is shown in **Figure 6e**. 1-CN treatment reduced the PV bandgap from 1.44 to 1.42 eV and lowered the E_{CT} from 1.36 to 1.38 eV. Specifically, the radiative loss (ΔE_r) was reduced by 0.02 eV by 1-CN owing to the higher EQE response but the non-radiative loss (ΔE_{nr}) increased by 0.02 eV. In brief, the 1-CN processed blend did not alleviate the energy loss. In contrast, 2-CN treatment reduced ΔE_r to 0.27 eV and maintained a low ΔE_{nr} of 0.20 eV, thus decreasing energy loss and boosting V_{OC}.

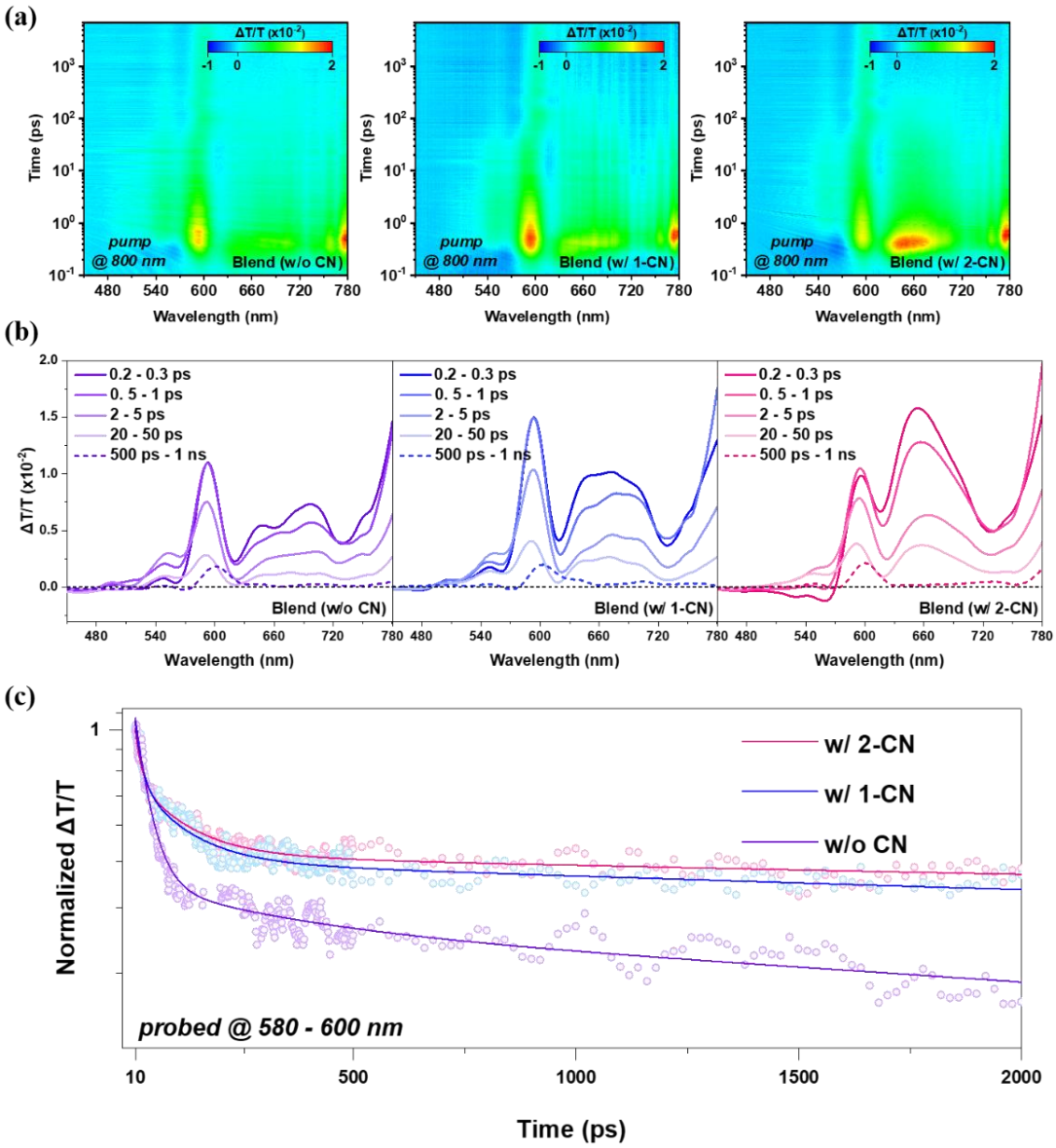

Figure 7. Transient absorption spectra (TAS) analysis: (a) 2D contour map of TAS results for D18-Fu:L8-BO blend films treated by three ways and (b) the corresponding

representative absorption profiles at typical time. (c) Decay kinetics fitting for them.

In-depth photophysical property analysis was conducted via transient absorption spectra (TAS).[58-61] **Figures 7** and **S5** include all testing results and analysis of D18-Fu/L8-BO neat films and their blend systems processed in three different ways. First, a 400 nm pump was used to screen the features of the polymer donor, while an 800 nm pump was used for L8-BO detection. It is noted that in the range of 580–600 nm, L8-BO has no feature peaks but D18-Fu exhibits a significant photobleaching peak that represents hole polaron behaviors. Accordingly, the blend film (excited at 800 nm) was investigated out based on fitting for this region. The rise of the ground state bleaching peaks of both CN-treated films implies boosted charge transfer and thus charge generation, which is consistent with the *J-V* and EQE curves. In the sub-nanosecond regime, the decay fitting referring to bimolecular recombination demonstrates the significant effect of suppression for CN treatment, which enables *FF* enhancements. Meanwhile, the slightly slower decay of the 2-CN film indicates a marginally higher *FF* than the the 1-CN system. In addition, the reduced recombination of the 2-CN processed film also supports the lower energy loss in solar cells.

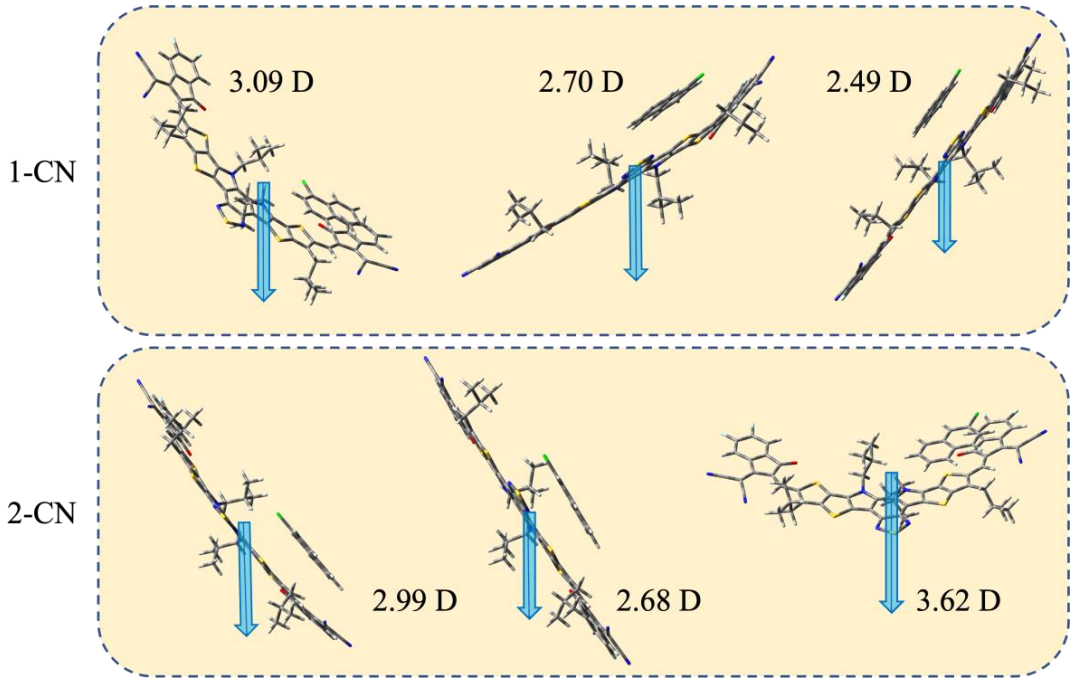

Figure 8. Calculated dipole moments of the three most stable CN:acceptor dimers for

each additive in chloroform.

Theoretical simulations were performed to investigate the molecular nature of the active layer. DFT simulation of a single molecule (**Figures S6-S9**) revealed that CN (1-CN or 2-CN) may interact with the whole backbone of the donor or acceptor. A rotamer scan of the donor monomer (**Figure S9**) showed that D18-Fu prefers to maintain a planar configuration, while the energy barrier of rotating is approximately 3.5 kcal/mol. Molecular dynamics simulations at the GFN2-xTB level[62] of CN:donor-unit or CN:acceptor dimers showed that CN would shift along the backbone for both combinations of dimers in over 30 simulations. For the dimer of the CN:D18-Fu unit, CN was prone to stay near the BDF unit, while for the dimer of CN:L8-BO, it was not clear which site CN preferred to stay with L8-BO since the number of samples was small. Additionally, CN prefered to stick to the backbone by π-π interactions. However, the interaction between CN and the active layer showed no difference during molecular dynamics simulation. To further study the difference between CN, we optimized over 70 CN:donor-unit or CN:acceptor dimer structures using the DFT method (**Figure S10**). In the CN:donor complex, CN preferred to stick to the BDF unit, which was about 2 to 2.5 kcal/mol more stable than other positions. In the CN:acceptor complex, CN was mainly located around the double bond and outer thiophene. The dipole moments were calculated using the def2-SVPD basis set,[63] since there is a huge difference between the dipole moment directions calculated with the 6-31G(d) and 6-311+G(d) basis for the same structure. In chloroform, the L8-BO molecule had almost no dipole moment (0.21 D). After complexation with additives, both 1-CN and 2-CN increased the induced dipole moment of L8-BO. Since chloroform is a weakly polar solvent, increasing the dipole moment of L8-BO would help separate it from chloroform. Therefore, the aggregation and crystallization of L8-BO was accelerated. **Figure 8** presented the three most stable CN:acceptor dimers, among which the 2-CN:L8-BO dimer exhibits a larger induced dipole moment (3.62 D) than 1-CN:L8-BO (3.09 D). In conclusion, 1-CN and 2-CN increased the dipole moment of L8-BO and enhanced molecular aggregation. In addition, 2-CN facilitated faster nucleation and

crystallization of the acceptor than 1-CN, which is consistent with the re *in-situ* UV-vis absorption and GIWAXS results.

Beyond the typical D18-Fu: L8-BO system, the isomeric solid additive strategy was applied to two other known systems, namely PM6:Y6 and PM6:PY-IT.[64-67] Both were optimized by 1-CN and produced milestone PCEs for OSCs and all-polymer solar cells. We compared their PV performances using 1-CN and 2-CN to ascertain the applicability of this method. The chemical structures of these materials and the corresponding *J-V* characteristics and EQE spectra of the optimal devices are shown in **Figure S11** and the device parameters and 2-CN ratio optimization data are presented in **Tables S5** and **S6**. 2-CN performed better than 1-CN for both systems; however, PCE was enhanced less than in the D18-Fu:L8-BO system and the PV parameters were tuned differently. The aggregation property of PM6 and its interaction with liquid or solid isomeric CN additives differed from those of D18-Fu. Therefore, the general applicability of this method and its particular suitability with the D18-Fu:L8-BO system were proven.

Conclusion

An efficiency breakthrough for BDF-based polymer donors via device engineering was realized. We employed a recent high-performance BDF donor (D18-Fu) and combined it with L8-BO, whose morphology was optimized using 2-CN as the solvent additive, to achieve a PCE of 18.4%, a record for BDF polymers. The morphology formation process was studied in detail using in situ techniques and the working mechanism of 2-CN, as compared with its popular isomer, 1-CN, was comprehensively investigated through morphology and device characterizations. We also demonstrated that 2-CN could enhance the PCE of PM6:Y6 and PM6:PY-IT, suggesting that 2-CN can be explored as a general solvent additive like 1-CN; however, its morphology regulation mechanism is drastically different from that of 1-CN. The major contributions of this study are indicating the potential for not only D18-Fu but also other existing or upcoming BDF polymers and revealing the difference between isomeric CN additives in altering the morphology of different material systems. We

successfully showed that the synergy of rational material selection and morphology optimization is of great importance for the development of the OSC field, which could play an important role in material synthesis.

Acknowledgements

G. Zhang thanks the support from the Guangdong Basic and Applied Basic Research Foundation (2022A1515010875), Guangdong Basic and Applied Basic Research Foundation (2021A1515110017), Natural Science Foundation of Top Talent of SZTU (grant no. 20200205), and Project of Education Commission of Guangdong Province of China (2021KQNCX080). G. Li acknowledges the support from the Research Grants Council of Hong Kong (Project Nos 15221320, C5037-18G), RGC Senior Research Fellowship Scheme (SRFS2223-5S01), National Natural Science Foundation of China (51961165102), Shenzhen Science and Technology Innovation Commission (JCYJ20200109105003940), Hong Kong Polytechnic University Internal Research Funds: Sir Sze-yuen Chung Endowed Professorship Fund (8-8480), RISE (Q-CDA5), 1-W15V, 1-YW4C, and Guangdong-Hong Kong-Macao Joint Laboratory for Photonic-Thermal-Electrical Energy Materials and Devices (GDSTC No. 2019B121205001). H. Yan appreciates the support from the National Key Research and Development Program of China (No. 2019YFA0705900) funded by MOST, the Basic and Applied Research Major Program of Guangdong Province (No. 2019B030302007), the Shen Zhen Technology and Innovation Commission through (Shenzhen Fundamental Research Program, JCYJ20200109140801751), the Hong Kong Research Grants Council (research fellow scheme RFS2021-6S05, RIF project R6021-18, CRF project C6023-19G, GRF project 16310019, 16310020, 16309221, and 16309822), the Hong Kong Innovation and Technology Commission (ITC-CNERC14SC01), Foshan-HKUST (Project NO. FSUST19-CAT0202), Zhongshan Municipal Bureau of Science and Technology (NO.ZSST20SC02), and Tencent Xplorer Prize. R. Ma thanks the PolyU Distinguished Postdoctoral Fellowship (1-YW4C) for its support. Prof. Harald Ade is appreciated for acquiring the resonant soft X-ray scattering data.

Author Contributions

Lu Chen, Jicheng Yi, and Ruijie Ma contributed equally to this work.

Lu Chen: Investigation, Formal Analysis

Jicheng Yi: Investigation, Formal Analysis

Ruijie Ma: Conceptualization, Formal Analysis, Investigation, Writing-Original Draft, Supervision, Writing-Review and Editing, Project Administration

Lu Ding: Investigation, Formal Analysis

Top Archie Dela Peña: Investigation, Formal Analysis

Heng Liu: Investigation, Formal Analysis

Jian Chen: Investigation

Cuifen Zhang: Investigation, Formal Analysis

Chaoyue Zhao: Investigation

Wen Lu: Investigation

Qi Wei : Investigation

Bin Zhao: Resources

Zaifei Ma: Resources

Huawei Hu: Resources

Jiaying Wu: Resources

Xinhui Lu: Resources

Mingjie Li: Resources

Guangye Zhang: Resources, Supervision, Funding Acquisition, Writing-Review & Editing.

Gang Li: Resources, Supervision, Funding Acquisition

He Yan: Resources, Supervision, Funding Acquisition

References

[1] A. E. Steen, T. L. Ellington, S. T. Nguyen, S. Balasubramaniam, I. Chandrasiri, J. H. Delcamp, G. S. Tschumper, N. I. Hammer, D. L. Watkins, *J Phys Chem C* **2019**, *123*, 15176.

[2] O. Gidron, A. Dadvand, Y. Sheynin, M. Bendikov, D. F. Perepichka, *Chem. Commun.* **2011**, *47*, 1976.

[3] L. Zhu, M. Zhang, J. Xu, C. Li, J. Yan, G. Zhou, W. Zhong, T. Hao, J. Song, X. Xue, Z. Zhou, R. Zeng, H. Zhu, C.-C. Chen, R. C. I. MacKenzie, Y. Zou, J. Nelson, Y. Zhang, Y. Sun, F. Liu, *Nat.*

Mater. **2022**, *21*, 656.
[4] Y. Cui, Y. Xu, H. Yao, P. Bi, L. Hong, J. Zhang, Y. Zu, T. Zhang, J. Qin, J. Ren, Z. Chen, C. He, X. Hao, Z. Wei, J. Hou, *Adv. Mater.* **2021**, *33*, 2102420.
[5] J. Wang, M. Zhang, J. Lin, Z. Zheng, L. Zhu, P. Bi, H. Liang, X. Guo, J. Wu, Y. Wang, L. Yu, J. Li, J. Lv, X. Liu, F. Liu, J. Hou, Y. Li, *Energy Environ. Sci.* **2022**, *15*, 1585.
[6] R. Ma, C. Yan, P. W.-K. Fong, J. Yu, H. Liu, J. Yin, J. Huang, X. Lu, H. Yan, G. Li, *Energy Environ. Sci.* **2022**, *15*, 2479.
[7] Y. Wei, Z. Chen, G. Lu, N. Yu, C. Li, J. Gao, X. Gu, X. Hao, G. Lu, Z. Tang, J. Zhang, Z. Wei, X. Zhang, H. Huang, *Adv. Mater.* **2022**, *34*, 2204718.
[8] Q. Fan, R. Ma, Z. Bi, X. Liao, B. Wu, S. Zhang, W. Su, J. Fang, C. Zhao, C. Yan, K. Chen, Y. Li, C. Gao, G. Li, W. Ma, *Adv. Funct. Mater.* **2023**, 33, 2211385.
[9] J. Wan, Y. Wu, R. Sun, J. Qiao, X. Hao, J. Min, *Energy Environ. Sci.* **2022**, *15*, 5192.
[10] X. Li, X. Duan, Z. Liang, L. Yan, Y. Yang, J. Qiao, X. Hao, C. Zhang, J. Zhang, Y. Li, F. Huang, Y. Sun, *Adv. Energy Mater.* **2022**, *12*, 2103684.
[11] J. Yi, M. Pan, L. Chen, Y. Chen, I. C. Angunawela, S. Luo, T. Zhang, A. Zeng, J. Chen, Z. Qi, H. Yu, W. Liu, J. Y. L. Lai, H. K. Kim, X. Zhu, H. Ade, H. Lin, H. Yan, *Adv. Energy Mater.* **2022**, *12*, 2201850.
[12] B. Zheng, J. Ni, S. Li, Y. Yue, J. Wang, J. Zhang, Y. Li, L. Huo, *Adv. Sci.* **2022**, *9*, 2105430.
[13] B. Liu, H. Sun, J.-W. Lee, J. Yang, J. Wang, Y. Li, B. Li, M. Xu, Q. Liao, W. Zhang, D. Han, L. Niu, H. Meng, B. J. Kim, X. Guo, *Energy Environ. Sci.* **2021**, *14*, 4499.
[14] S. Bao, H. Yang, H. Fan, J. Zhang, Z. Wei, C. Cui, Y. Li, *Adv. Mater.* **2021**, *33*, 2105301.
[15] J. Fu, H. Chen, P. Huang, Q. Yu, H. Tang, S. Chen, S. Jung, K. Sun, C. Yang, S. Lu, Z. Kan, Z. Xiao, G. Li, *Nano Energy* **2021**, *84*, 105862.
[16] Y. Zhang, Y. Cho, J. Lee, J. Oh, S.-H. Kang, S. M. Lee, B. Lee, L. Zhong, B. Huang, S. Lee, J.-W. Lee, B. J. Kim, Y. Li, C. Yang, *J. Mater. Chem. A* **2020**, *8*, 13049.
[17] R. Ma, C. Yan, J. Yu, T. Liu, H. Liu, Y. Li, J. Chen, Z. Luo, B. Tang, X. Lu, G. Li, H. Yan, *ACS Energy Lett.* **2022**, *7*, 2547.
[18] X. Song, K. Zhang, R. Guo, K. Sun, Z. Zhou, S. Huang, L. Huber, M. Reus, J. Zhou, M. Schwartzkopf, S. V. Roth, W. Liu, Y. Liu, W. Zhu, P. Müller-Buschbaum, *Adv. Mater.* **2022**, *34*, 2200907.
[19] S.-H. Bae, H.g Zhao, Y.-T. Hsieh, L. Zuo, N. D. Marco, Y. S. Rim, G. Li, Y. Yang,. *Chem* **2016**, *1*, 197.
[20] Y. Zhang, K. Liu, J. Huang, X. Xia, J. Cao, G. Zhao, P. W.K. Fong, Y. Zhu, F. Yan, Y. Yang, X. Lu, Gang Li, *Nat. Commun*. **2021**, *12*, 4815.
[21] Y Zhang, Y. Lang, G. Li, *EcoMat* **2023**, *5*, e12281.
[22] J. Song, Y. Li, Y. Cai, R. Zhang, S. Wang, J. Xin, L. Han, D. Wei, W. Ma, F. Gao, Y. Sun, *Matter* **2022**, *5*, 4047.
[23] C. Li, J. Zhou, J. Song, J. Xu, H. Zhang, X. Zhang, J. Guo, L. Zhu, D. Wei, G. Han, J. Min, Y. Zhang, Z. Xie, Y. Yi, H. Yan, F. Gao, F. Liu, Y. Sun, *Nat. Energy* **2021**, *6*, 605.
[24] R. Yu, H. Yao, Y. Xu, J. Li, L. Hong, T. Zhang, Y. Cui, Z. Peng, M. Gao, L. Ye, Z. a. Tan, J. Hou, *Adv. Funct. Mater.* **2021**, *31*, 2010535.
[25] Z. Li, Y. Liang, X. Qian, L. Ying, Y. Cao, *Chem. Eng. J.* **2022**, *446*, 136877.
[26] C. McDowell, M. Abdelsamie, M. F. Toney, G. C. Bazan, *Adv. Mater.* **2018**, *30*, 1707114.
[27] R. Ma, M. Zeng, Y. Li, T. Liu, Z. Luo, Y. Xu, P. Li, N. Zheng, J. Li, Y. Li, R. Chen, J. Hou, F.

Huang, H. Yan, *Adv. Energy Mater.* **2021**, *11*, 2100492.
[28] B. Liu, H. Sun, J.-W. Lee, Z. Jiang, J. Qiao, J. Wang, J. Yang, K. Feng, Q. Liao, M. An, B. Li, D. Han, B. Xu, H. Lian, L. Niu, B. J. Kim, X. Guo, *Nat. Commun.* **2023**, 14, 967.
[29] R. Ma, Q. Fan, T. A. Dela Peña, B. Wu, H. Liu, Q. Wu, Q. Wei, J. Wu, X. Lu, M. Li, W. Ma, G. Li, *Adv. Mater.* **2023**, n/a, 2212275.
[30] Z. Luo, Y. Gao, H. Lai, Y. Li, Z. Wu, Z. Chen, R. Sun, J. Ren, C. e. Zhang, F. He, H. Woo, J. Min, C. Yang, *Energy Environ. Sci.* **2022**, 15, 4601.
[31] T. Wang, J.-L. Brédas, *J Am Chem Soc.* **2021**, *143*, 1822.
[32] J. J. van Franeker, M. Turbiez, W. Li, M. M. Wienk, R. A. J. Janssen, *Nat. Commun.* **2015**, *6*, 6229.
[33] B. Lin, X. Zhou, H. Zhao, J. Yuan, K. Zhou, K. Chen, H. Wu, R. Guo, M. A. Scheel, A. Chumakov, S. V. Roth, Y. Mao, L. Wang, Z. Tang, P. Müller-Buschbaum, W. Ma, *Energy Environ. Sci.* **2020**, *13*, 2467.
[34] Q. Bai, Q. Liang, H. Li, H. Sun, X. Guo, L. Niu, *Aggregate* **2022**, *3*, e281.
[35] C. Guo, D. Li, L. Wang, B. Du, Z.-X. Liu, Z. Shen, P. Wang, X. Zhang, J. Cai, S. Cheng, C. Yu, H. Wang, D. Liu, C.-Z. Li, T. Wang, *Adv. Energy Mater.* **2021**, *11*, 2102000.
[36] R. Ma, T. Yang, Y. Xiao, T. Liu, G. Zhang, Z. Luo, G. Li, X. Lu, H. Yan, B. Tang, *Energy Environ. Mater.* **2022**, 5, 977.
[37] L. Zhong, S.-H. Kang, J. Oh, S. Jung, Y. Cho, G. Park, S. Lee, S.-J. Yoon, H. Park, C. Yang, *Adv. Funct. Mater.* **2022**, 32, 2201080.
[38] Q. V. Hoang, S. Rasool, S. Oh, D. Van Vu, D. H. Kim, H. K. Lee, C. E. Song, S. K. Lee, J.-C. Lee, S.-J. Moon, W. S. Shin, *J Mater Chem C* **2017**, 5, 7837.
[39] H. Zhao, B. Lin, J. Xue, H. B. Naveed, C. Zhao, X. Zhou, K. Zhou, H. Wu, Y. Cai, D. Yun, Z. Tang, W. Ma, *Adv. Mater.* **2022**, 34, 2105114.
[40] H. Chen, R. Zhang, X. Chen, G. Zeng, L. Kobera, S. Abbrent, B. Zhang, W. Chen, G. Xu, J. Oh, S.-H. Kang, S. Chen, C. Yang, J. Brus, J. Hou, F. Gao, Y. Li, Y. Li, *Nat. Energy* **2021**, 6, 1045.
[41] Y. Zhang, K. Liu, J. Huang, X. Xia, J. Cao, G. Zhao, P. W. K. Fong, Y. Zhu, F. Yan, Y. Yang, X. Lu, G. Li, *Nat. Commun.* **2021**, 12, 4815.
[42] D. Jeong, G.-U. Kim, D. Lee, S. Seo, S. Lee, D. Han, H. Park, B. Ma, S. Cho, B. J. Kim, *Adv. Energy Mater.* **2022**, 12, 2201603.
[43] L. Zhu, M. Zhang, W. Zhong, S. Leng, G. Zhou, Y. Zou, X. Su, H. Ding, P. Gu, F. Liu, Y. Zhang, *Energy Environ. Sci.* **2021**, 14, 4341.
[44] J. Xue, H. Zhao, B. Lin, Y. Wang, Q. Zhu, G. Lu, B. Wu, Z. Bi, X. Zhou, C. Zhao, G. Lu, K. Zhou, W. Ma, *Adv. Mater.* **2022**, 34, 2202659.
[45] T. Fritsch, J. Kurpiers, S. Roland, N. Tokmoldin, S. Shoaee, T. Ferron, B. A. Collins, S. Janietz, K. Vandewal, D. Neher, *Adv. Energy Mater.* **2022**, 12, 2200641.
[46] Y. Gu, C. Wang, T. P. Russell, *Adv. Energy Mater.* **2012**, 2, 683.
[47] J. Rivnay, S. C. B. Mannsfeld, C. E. Miller, A. Salleo, M. F. Toney, *Chem. Rev.* **2012**, 112, 5488.
[48] R. Ma, K. Zhou, Y. Sun, T. Liu, Y. Kan, Y. Xiao, T. A. Dela Peña, Y. Li, X. Zou, Z. Xing, Z. Luo, K. S. Wong, X. Lu, L. Ye, H. Yan, K. Gao, *Matter* **2022**, 5, 725.
[49] T. Liu, K. Zhou, R. Ma, L. Zhang, C. Huang, Z. Luo, H. Zhu, S. Yao, C. Yang, B. Zou, L. Ye, *Aggregate* **2022**, n/a, e308.
[50]. X. Jiang, P. Chotard, K. Luo, F. Eckmann, S. Tu, M. A. Reus, S. Yin, J. Reitenbach, C. L.

Weindl, M. Schwartzkopf, S. V. Roth, P. Müller-Buschbaum, *Adv. Energy Mater.* **2022**, 12, 2103977.
[51] W. Gao, M. Jiang, Z. Wu, B. Fan, W. Jiang, N. Cai, H. Xie, F. R. Lin, J. Luo, Q. An, H. Y. Woo, A. K. Y. Jen, *Angew. Chem. Int. Ed.* **2022**, 61, e202205168.
[52] T. Xiao, J. Wang, S. Yang, Y. Zhu, D. Li, Z. Wang, S. Feng, L. Bu, X. Zhan, G. Lu, *J. Mater. Chem. A* **2020**, 8, 401.
[53] C. Zhao, R. Ma, J. Oh, L. Wang, G. Zhang, Y. Wang, S. He, L. Zhu, C. Yang, G. Zhang, G. Li, *J Mater Chem C* **2022**, 10, 17899.
[54] Y. Cai, Q. Li, G. Lu, H. S. Ryu, Y. Li, H. Jin, Z. Chen, Z. Tang, G. Lu, X. Hao, H. Y. Woo, C. Zhang, Y. Sun, *Nat. Commun.* **2022**, 13, 2369.
[55] Y. Wang, D. Qian, Y. Cui, H. Zhang, J. Hou, K. Vandewal, T. Kirchartz, F. Gao, *Adv. Energy Mater.* **2018**, 8, 1801352.
[56] O. Almora, C. I. Cabrera, J. Garcia-Cerrillo, T. Kirchartz, U. Rau, C. J. Brabec, *Adv. Energy Mater.* **2021**, 11, 2100022.
[57] Z. Luo, R. Ma, J. Yu, H. Liu, T. Liu, F. Ni, J. Hu, Y. Zou, A. Zeng, C.-J. Su, U. S. Jeng, X. Lu, F. Gao, C. Yang, H. Yan, *Nati. Sci. Rev.* **2022**, 9, nwac076.
[58] L. Yan, Z. Liang, J. Si, P. Gong, Y. Wang, X. Liu, J. Tong, J. Li, X. Hou, *ACS Applied Materials & Interfaces* **2022**, 14, 6945.
[59] T. A. Dela Peña, J. I. Khan, N. Chaturvedi, R. Ma, Z. Xing, J. Gorenflot, A. Sharma, F. L. Ng, D. Baran, H. Yan, F. Laquai, K. S. Wong, *ACS Energy Lett.* **2021**, 6, 3408.
[60] T. Huo, L. Yan, J. Si, P. Ma, X. Hou, *Journal of Materials Chemistry C* **2023**, DOI: 10.1039/D2TC03632K.
[61] C. Wang, L. Yan, J. Si, T. Huo, X. Hou, *J. Alloys Compd.* **2023**, DOI: https://doi.org/10.1016/j.jallcom.2023.169272169272.
[62] C. Bannwarth, S. Ehlert, S. Grimme, *J. Chem. Theory Comput*. **2019**, 15, 1652.
[63] J. C. Zapata, L. K. McKemmish, *J. Phys. Chem. A* **2020**, 124, 7538.
[64] J. Yuan, Y. Zhang, L. Zhou, G. Zhang, H.-L. Yip, T.-K. Lau, X. Lu, C. Zhu, H. Peng, P. A. Johnson, M. Leclerc, Y. Cao, J. Ulanski, Y. Li, Y. Zou, *Joule* **2019**, 3, 1140.
[65] Z. Luo, T. Liu, R. Ma, Y. Xiao, L. Zhan, G. Zhang, H. Sun, F. Ni, G. Chai, J. Wang, C. Zhong, Y. Zou, X. Guo, X. Lu, H. Chen, H. Yan, C. Yang, *Adv. Mater.* **2020**, 32, 2005942.
[66] L. Zhan, S. Li, Y. Li, R. Sun, J. Min, Y. Chen, J. Fang, C.-Q. Ma, G. Zhou, H. Zhu, L. Zuo, H. Qiu, S. Yin, H. Chen, *Adv. Energy Mater.* **2022**, *12*, 2201076.
[67] Q. Fan, R. Ma, W. Su, Q. Zhu, Z. Luo, K. Chen, Y. Tang, F. R. Lin, Y. Li, H. Yan, C. Yang, A. K. Y. Jen, W. Ma, *Carbon Energy* **2023**, 5, e267.